Hindawi Publishing Corporation
Mathematical Problems in Engineering
Volume 2014, Article ID 653208, 12 pages
http://dx.doi.org/10.1155/2014/653208

Research Article

Sparse Scenario Imaging for Active Radar in the Forward-Looking Direction

Jun Wang, Fenggang Yan, Yinan Zhao, and Xiaolin Qiao

School of Electronics and Information Engineering, Harbin Institute of Technology, Harbin, Heilongjiang 150001, China

Correspondence should be addressed to Jun Wang; johnwangstudio@gmail.com

Received 8 April 2014; Accepted 29 May 2014; Published 3 July 2014

Academic Editor: Caner Özdemir

The resolution of multiple targets at the same range cell but different angles in the forward-looking direction is of great trouble for active radar. Based on compressive sensing (CS) framework, a sparse scenario imaging approach using joint angle-Doppler representation basis is proposed, which employs multisensor and single-receiver channel hardware architecture. Firstly, the joint angle-Doppler representation basis is formulated using the Doppler dictionary, and then the radar returns during multiple pulse repetition periods are modeled as the measurements with respect to a stationary sparse target scenario via the joint representation basis; in the end, the image of sparse target scenario is recovered using the single-receiver echoes. Numerical experiments demonstrate that the proposed method can provide an image of the spatial sparse scenario at the same range for active radar in the forward-looking direction.

1. Introduction

In the forward-looking direction, the resolution of multiple targets at the same range cell but different angles is of great trouble for active radar because traditional Doppler beam sharpening (DBS) and synthetic aperture radar (SAR) techniques can be employed to improve the cross-range resolution only in the squint and side-looking direction. Conventional multiple signal classification (MUSIC) and estimation of signal parameters via rotational invariance techniques (ESPRIT) algorithms which can obtain direction-of-arrival (DOA) of multiple targets can be difficultly employed in active radar because of the need of multireceiver structure and the decayed performance with coherent signals circumstance.

Compressive sensing (CS) [1, 2] is emerged in the past few years which states that a sparse signal can be economically acquired in a more economical way. A signal $\mathbf{x} \in \mathbb{C}^N$ which can be written in $\mathbf{x} = \mathbf{\Psi s}$ where $\mathbf{\Psi}$ is a representation basis is defined as a K-sparse signal if the number of nonzero elements of vector $\mathbf{s}$ is not larger than K. CS suggests that the sparse signal $\mathbf{x}$ can be reconstructed using $M \ll N$ measurements $\mathbf{y} = \mathbf{\Phi x} + \mathbf{n}$ if equivalent dictionary $\mathbf{D} = \mathbf{\Phi\Psi}$ satisfies RIP [1], where $\mathbf{\Phi} \in \mathbb{C}^{M\times N}$ is the measurement matrix and $\mathbf{n} \in \mathbb{C}^M$ is additive noise. The reconstructed $\hat{\mathbf{x}}$ can be obtained by solving a convex optimization problem as follows:

$$\min_{\hat{\mathbf{s}}\in\mathbb{C}^N} \|\hat{\mathbf{s}}\|_1, \quad \text{s.t. } \|\mathbf{y} - \mathbf{D}\hat{\mathbf{s}}\|_2 \le \varepsilon, \tag{1}$$

where $\varepsilon = \|\mathbf{n}\|_2$ and $\|\cdot\|_p$ denotes ℓp-norm.

DOA estimation problem generally faces a sparse target scenario in the spatial domain; consequently the application of CS in DOA estimation has been concerned recently. In [3, 4], DOA estimation is modeled as single measurement vector problem (SMV) and, in [5, 6], is solved using joint sparse reconstruction algorithm SOMP [7] based on multiple measurement vector model (MMV) [8]. Numerical experiments show that the DOA estimation algorithms based on CS exhibit better performance than traditional subspace algorithms such as MUSIC and ESPRIT, especially at lower signal-to-noise ratio (SNR) and with coherent signal circumstance. Inspired by Bayesian CS [9] and MT-CS [10] framework, [11–13] provide more accurate DOA estimation than traditional algorithms using appropriate priors with respect to hyperparameters. The compressive MUSIC [14] can approach

the optimal l_0-bound with finite number of snapshots even in cases where the signals are linear dependent. In [15], an SAR image compression approach based on CS shows better performance on preserving the important features than JPEG and JPEG2000, and the CS TomoSAR theory in [16] has superresolution properties and point localization accuracies.

Motivated by the better performance in DOA estimation and cross-range resolution in SAR based on CS framework, we develop a sparse scenario imaging strategy for active radar in the forward-looking direction which employs multisensor single-receiver channel structure.

2. Measurement Model of Sparse Scenario

In this section, the measurement model with respect to sparse target scenario is presented based on the joint angle-Doppler representation basis.

Traditional DOA estimation algorithms such as MUSIC and ESPRIT exploit relative phases between the outputs of multiple array sensors to determine multiple targets. In the proposed strategy, multiple equivalent sensors are formed in phased array radar (PAR) in order to provide a multisensor output during the reception. In nature, each equivalent sensor is a subarray which consists of multiple array elements. As shown in Figure 1, PAR forms M beams pointing to target scenario Ω using M subarrays during the reception and only one beam for illumination. The phase centers of M equivalent sensors can be expressed as $(x_m, y_m, 0)$, $m = 0, \ldots, M-1$.

2.1. Measurement Model Using Multisensor. As depicted in Figure 2, the interest spatial area is restricted in elevation $\theta_{\max}$ and is discretized into N spatial grids $\Omega = \{\mathbf{u}_n, n = 0, \ldots, N-1\}$, where $\mathbf{u}_n = [u_n, v_n, w_n]^T$ is the cosine vector corresponding to nth grid which has elevation angle θ_n and azimuth angle φ_n.

Assuming that the radar is moving to Ω along with z axis as shown in Figure 2, let $\hat{t}$ denote fast time, and let $t_r = rT_r$ denote rth slow time where T_r is pulse repetition interval (PRI), and then the full time $t = t_r + \hat{t}$ is abbreviated to $(\hat{t}, t_r)$. The illumination waveform is $p(\hat{t}) = R(\hat{t})\tilde{p}(\hat{t})$, where $R(\hat{t}) = 1$, $0 \le \hat{t} \le \tau$; $R(\hat{t}) = 0$, $\hat{t} > \tau$, is a window function and $\tilde{p}(\hat{t})$ is a wideband waveform. For simplicity, let $(\hat{t}, \mathbf{u}_n)$ denote the target position in nth spatial grid $\mathbf{u}_n$ at the range cell $\hat{t}$. Due to noncooperation property of target for active radar, the corresponding Doppler is not a prior. With respect to an arbitrary target on $(\hat{t}_T, \mathbf{u}_n)$, the returns of the reference array sensor whose coordinate is $(0, 0, 0)$ in one observation period including R PRIs can be expressed as follows:

$$\beta_n(\hat{t}_T)\, p(\hat{t} - \hat{t}_T) \exp\left[j2\pi f_n(\hat{t} + t_r)\right], \quad r = 0, \ldots, R-1, \tag{2}$$

where $\beta_n(\hat{t}_T)$ is the amplitude of target on $(\hat{t}_T, \mathbf{u}_n)$, and f_n is the corresponding unknown Doppler. The subscript "n" of $\beta_n(\hat{t}_T)$ and f_n denotes the corresponding term about the target from the nth spatial grid $\mathbf{u}_n \in \Omega$.

A sparse target scenario $E = \{(\hat{t}_T, \mathbf{u}_n), \mathbf{u}_n \in T\}$ where $K \ll N$ targets are located in $T \subset \Omega$ at the same range cell $\hat{t}_T$ is considered, where $T = \{\mathbf{u}_n, n \in I_T\}$ and I_T is the target index set of T in spatial domain Ω. The index set I_T satisfies the equation $|\operatorname{supp}(I_T)| = K$, where $\operatorname{supp}(\cdot)$ denotes the support operation and $|\cdot|$ denotes the element number of set. It is of great trouble for traditional active radar to determine such a target scenario in the forward-looking direction.

In order to express the radar returns from target scenario E, the Doppler dictionary $F = \{f_s^d\}_{s=0}^{S-1}$ including $S \ge K$ frequencies is employed here to settle the unknown Doppler problem in (2). The Doppler dictionary F can be seen as the estimation about the unknown target Doppler $F_D = \{f_n, n \in I_T\}$ of scenario E, and the estimated method will be given in Section 3. Due to the consideration on estimation error, we assume that there are more frequencies in F than actual Doppler assemble F_D; that is, $S \ge K$. Based on the utilization of F, we only "know" the estimated Doppler frequencies about scenario E, but we "do not know" the relationship between the frequencies f_s^d, $s = 0, \ldots, S-1$ in F and target directions $\mathbf{u}_n$, $n \in I_T$ in T. Therefore, an amplitude vector $\boldsymbol{\beta}_n(\hat{t}_T) = [\beta_{n,0}(\hat{t}_T), \ldots, \beta_{n,S-1}(\hat{t}_T)]^T$ corresponding to all S frequencies in F is defined for the target located in arbitrary nth grid $\mathbf{u}_n$, where the sth element of $\beta_{n,s}(\hat{t}_T)$, $s = 0, \ldots, S-1$, denotes the amplitude when the Doppler of the target in $\mathbf{u}_n$ is the sth frequency $f_s^d \in F$, $s = 0, \ldots, S-1$. Assuming that the actual Doppler f_n of the target in $\mathbf{u}_n$ is equal to the ith frequency $f_i^d \in F$, the corresponding ith element $\beta_{n,i}(\hat{t}_T)$ in amplitude vector $\boldsymbol{\beta}_n(\hat{t}_T)$ denotes the actual target amplitude which is nonzero; however, other elements in $\boldsymbol{\beta}_n(\hat{t}_T)$, that is, $\beta_{n,s}(\hat{t}_T)$, $s \ne i$, $0 \le s \le S-1$, are zeros because the target Doppler is not equal to the frequencies $f_s^d \in F$, $s \ne i$, $0 \le s \le S-1$. In a word, if the actual Doppler of target on $(\hat{t}_T, \mathbf{u}_n)$ corresponds to the ith frequency in F, that is, $f_n = f_i^d$, the amplitude vector $\boldsymbol{\beta}_n(\hat{t}_T)$ satisfies

$$\begin{aligned} \left|\beta_{n,s}(\hat{t}_T)\right| &\ne 0, \quad s = i, \\ \left|\beta_{n,s}(\hat{t}_T)\right| &= 0, \quad s \ne i,\ 0 \le s \le S-1. \end{aligned} \tag{3}$$

According to (3), there is not more than one nonzero element in $\boldsymbol{\beta}_n(\hat{t}_T)$; that is, $\|\boldsymbol{\beta}_n(\hat{t}_T)\|_0 \le 1$.

Regarding sparse scenario E, a sparse amplitude vector $\boldsymbol{\beta}(\hat{t}_T) = [\boldsymbol{\beta}_0^T(\hat{t}_T), \ldots, \boldsymbol{\beta}_{N-1}^T(\hat{t}_T)]^T \in \mathbb{C}^{SN}$ defined on joint angle-Doppler domain $\Omega \otimes F$ is employed, where "$\otimes$" denotes direct product. The nth element, $\boldsymbol{\beta}_n^T(\hat{t}_T)$, $n = 0, \ldots, N-1$, in $\boldsymbol{\beta}(\hat{t}_T)$ denotes the amplitude for the target in the nth grid $\mathbf{u}_n \in \Omega$. If there actually exists a target in the nth grid, that is, $\mathbf{u}_n \in T$, its amplitude being $\boldsymbol{\beta}_n^T(\hat{t}_T)$, $n \in I_T$ satisfies (3); otherwise, the amplitude vectors $\boldsymbol{\beta}_n^T(\hat{t}_T)$, $n \notin I_T$, $n = 0, \ldots, N-1$, are equal to zero because there is not an actual target. Omitting the fast time term $\hat{t}_T$, we abbreviate $\boldsymbol{\beta}_n(\hat{t}_T)$ to $\boldsymbol{\beta}_n = [\beta_{n,0}, \ldots, \beta_{n,S-1}]^T$, $n = 0, \ldots, N-1$ and $\boldsymbol{\beta}(\hat{t}_T)$ to $\boldsymbol{\beta} = [\boldsymbol{\beta}_0^T, \ldots, \boldsymbol{\beta}_{N-1}^T]^T$. The amplitude vector $\boldsymbol{\beta}$ is also named as sparse target scenario in the paper which is a "block-structure" vector as follows:

$$\boldsymbol{\beta} = \left[\underbrace{\beta_{0,0}, \ldots, \beta_{0,S-1}}_{\text{block } 0\#}, \ldots, \underbrace{\beta_{N-1,0}, \ldots, \beta_{N-1,S-1}}_{\text{block } (N-1)\#}\right]^T. \tag{4}$$

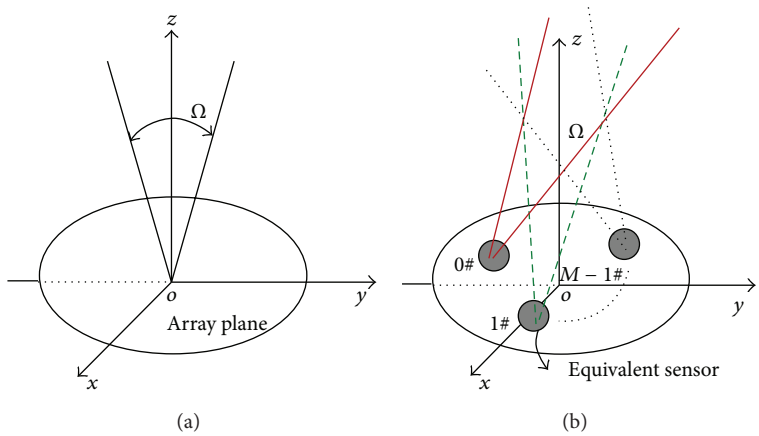

Figure 1: Illumination and receiving beam. (a) Illumination mode. (b) Receiving mode.

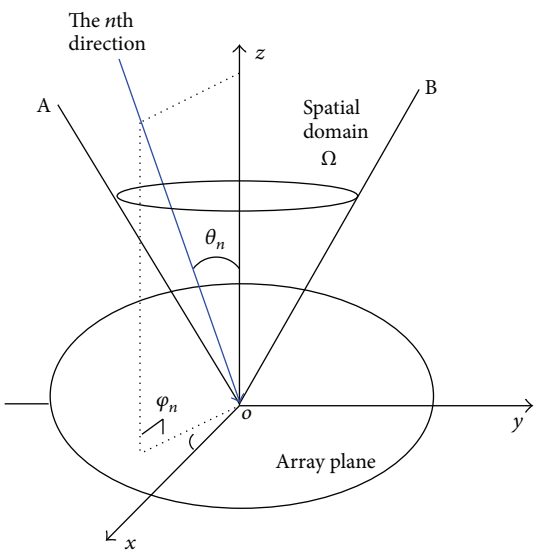

Figure 2: The geometry of array and target scenario.

The scenario $\boldsymbol{\beta}$ consists of N blocks in which each one has S elements. The nonzero element $\beta_{n,s} \in \boldsymbol{\beta}$, $n = 0, \ldots, N-1$; $s = 0, \ldots, S-1$ means that there is a target located in nth grid $\mathbf{u}_n$ and its Doppler is equal to sth frequency $f_s^d \in F$; otherwise, the zero element $\beta_{n,s} \in \boldsymbol{\beta}$ means that there is not a target corresponding to nth grid $\mathbf{u}_n$ and sth frequency $f_s^d \in F$. Therefore, there are not more than $\|\boldsymbol{\beta}\|_0 = K$ nonzero elements in $\boldsymbol{\beta}$ with respect to sparse scenario E.

With respect to an arbitrary target on $(\hat{t}_T, \mathbf{u}_n)$ with Doppler $f_s^d \in F$, the radar return of reference sensor $(0,0,0)$ during the reception of the rth PRI is

$$s_{n,s}^r(\hat{t}) = \beta_{n,s} p(\hat{t} - \hat{t}_T) \exp\left(j2\pi f_s^d \hat{t}\right) \exp\left(j2\pi f_s^d t_r\right), \quad (5)$$

where the superscript "r" corresponds to the rth PRT and the subscript "n, s" corresponds to the nth spatial grid $\mathbf{u}_n \in \Omega$ and the sth element $f_s^d \in F$. The receiving signal of the mth equivalent sensor about $\boldsymbol{\beta}$ which is assumed to be stationary during an observation period can be expressed as

$$y_m^r(\hat{t}) = \sum_{n=0}^{N-1} \sum_{s=0}^{S-1} s_{n,s}^r(\hat{t}) \cdot \exp\left[jk\left(u_n x_m + v_n y_m\right)\right], \quad (6)$$

where the subscript "m" represents the mth equivalent sensor and $k = 2\pi/\lambda$. The outputs of M equivalent sensors in the rth PRI can be shown as

$$\mathbf{y}^r(\hat{t}) = \mathbf{A} \times \mathbf{s}^r(\hat{t}), \quad (7)$$

where $\mathbf{y}^r(\hat{t}) = [y_0^r(\hat{t}), \ldots, y_{M-1}^r(\hat{t})]^T \in \mathbb{C}^M$ and $\mathbf{A} \in \mathbb{C}^{M \times SN}$ is the array response matrix about scenario $\boldsymbol{\beta}$ as follows:

$$\mathbf{A} = \left[\underbrace{\mathbf{a}_0, \ldots, \mathbf{a}_0}_{S} \ldots, \underbrace{\mathbf{a}_{N-1}, \ldots, \mathbf{a}_{N-1}}_{S}\right]. \quad (8)$$

There are N blocks in $\mathbf{A}$ and each block contains S identical steering vectors. The nth steering vector $\mathbf{a}_n$ in $\mathbf{A}$ is

$$\mathbf{a}_n = \left[a_{0,n}, \ldots, a_{M-1,n}\right]^T, \quad (9)$$

where $a_{m,n} = \exp[jk(u_n x_m + v_n y_m)]$, $m = 0, \ldots, M-1$. In (7), $\mathbf{s}^r(\hat{t}) \in \mathbb{C}^{SN}$ is the return of $\boldsymbol{\beta}$ at the full time $(\hat{t}, t_r)$:

$$\mathbf{s}^r(\hat{t}) = \boldsymbol{\beta} \odot \mathbf{p}(\hat{t} - \hat{t}_T) \odot \mathbf{e}^r, \quad (10)$$

where "$\odot$" denotes Hadamard product. In (10), $\mathbf{p}(\hat{t} - \hat{t}_T) \in \mathbb{C}^{SN}$ represents the part corresponding to fast time and $\mathbf{e}^r \in \mathbb{C}^{SN}$ represents the part corresponding to slow time of returns. If $\tilde{\mathbf{p}}(\hat{t} - \hat{t}_T) \in \mathbb{C}^S$ denotes the fast time term as shown in (5) which can be expressed as

$$\begin{aligned}\tilde{\mathbf{p}}(\hat{t} - \hat{t}_T) &= p(\hat{t} - \hat{t}_T)\left[\exp\left(j2\pi f_0^d \hat{t}\right), \ldots, \exp\left(j2\pi f_{S-1}^d \hat{t}\right)\right]^T \\ &= \left[\tilde{p}_0(\hat{t} - \hat{t}_T), \ldots, \tilde{p}_{S-1}(\hat{t} - \hat{t}_T)\right]^T,\end{aligned} \quad (11)$$

then $\mathbf{p}(\hat{t}-\hat{t}_T)$ is N repetition of $\tilde{\mathbf{p}}(\hat{t}-\hat{t}_T)$ as follows:

$$\mathbf{p}\left(\hat{t}-\hat{t}_T\right)=\left[\underbrace{\tilde{\mathbf{p}}^T\left(\hat{t}-\hat{t}_T\right),\ldots,\tilde{\mathbf{p}}^T\left(\hat{t}-\hat{t}_T\right)}_{N}\right]^T. \quad (12)$$

Similarly, the item $\mathbf{e}^r$ in (10) is N repetitions of $\tilde{\mathbf{e}}^r$ as follows:

$$\mathbf{e}^r=\left[\underbrace{(\tilde{\mathbf{e}}^r)^T,\ldots,(\tilde{\mathbf{e}}^r)^T}_{N}\right]^T, \quad (13)$$

where $\tilde{\mathbf{e}}^r=[\exp(j2\pi f_0^d t_r),\ldots,\exp(j2\pi f_{S-1}^d t_r)]^T$ is the item corresponding to the slow time in (5).

Substituting (12) and (13) into (7), the item in $\mathbf{s}^r(\hat{t})$ corresponding to slow time can be transferred to measurement matrix $\mathbf{A}$ and a new measurement model can be formulated as

$$\mathbf{y}^r\left(\hat{t}\right)=\mathbf{A}^r\times\mathbf{s}\left(\hat{t}\right), \quad (14)$$

where $\mathbf{s}(\hat{t})\in\mathbb{C}^{SN}$ stems from $\mathbf{s}^r(\hat{t})$ after eliminating the Doppler item $\mathbf{e}^r$, which is the return of $\boldsymbol{\beta}$ in the 0th PRI. The item $\mathbf{s}(\hat{t})$ is named as the return of $\boldsymbol{\beta}$ and can be expressed as

$$\begin{aligned}&\mathbf{s}\left(\hat{t}\right)\\&=\mathbf{s}^r(\hat{t})\big|_{r=0}=\boldsymbol{\beta}\odot\mathbf{p}\left(\hat{t}-\hat{t}_T\right)\\&=\left[\underbrace{s_{0,0}\left(\hat{t}\right),\ldots,s_{0,S-1}\left(\hat{t}\right)}_{\text{block }0\#},\ldots,\underbrace{s_{N-1,0}\left(\hat{t}\right),\ldots,s_{N-1,S-1}\left(\hat{t}\right)}_{\text{block }N-1\#}\right]^T.\end{aligned} \quad (15)$$

It is seen that $\mathbf{s}(\hat{t})$ is also a sparse signal which shares the same support as target scenario $\boldsymbol{\beta}$; therefore, $\mathbf{s}(\hat{t})$ is also regarded as sparse target scenario. The sth element in the nth block $s_{n,s}(\hat{t})$ of $\mathbf{s}(\hat{t})$, $n=0,\ldots,N-1$, $s=0\ldots,S-1$ denotes the return corresponding to nth target in Ω on sth Doppler of dictionary F at fast time $\hat{t}$. The matrix $\mathbf{A}^r\in\mathbb{C}^{M\times SN}$ in (14) stems from immigration of $\mathbf{e}^r$ to $\mathbf{A}$ based on (7), which is a joint angle-Doppler representation basis as follows:

$$\begin{aligned}&\mathbf{A}^r\\&=\left[\underbrace{e^{j2\pi f_0^d t_r}\mathbf{a}_0,\ldots,e^{j2\pi f_{S-1}^d t_r}\mathbf{a}_0}_{\text{block }0\#},\ldots,\underbrace{e^{j2\pi f_0^d t_r}\mathbf{a}_{N-1},\ldots,e^{j2\pi f_{S-1}^d t_r}\mathbf{a}_{N-1}}_{\text{block }N-1\#}\right].\end{aligned} \quad (16)$$

The matrix $\mathbf{A}^r$ also has a block-structure, and there are N blocks in which each block has S columns. In the arbitrary nth block of $\mathbf{A}^r$, $n=0,\ldots,N-1$, the same one steering vector $\mathbf{a}_n$ provides a representation in spatial angle domain for the response of receiving array including M equivalent sensors, and the items $\exp(j2\pi f_s^d t_r)$, $s=0,\ldots,S-1$ provide the representation for the phases in Doppler domain with respect to S Doppler frequencies f_s^d, $s=0,\ldots,S-1$. Consequently, $\mathbf{A}^r$ is a representation for the return of target scenario $\boldsymbol{\beta}$ in joint angle-Doppler domain.

According to (7) and (14), the measurement $\mathbf{y}^r(\hat{t})$ about the return $\mathbf{s}^r(\hat{t})$ of $\boldsymbol{\beta}$ in arbitrary rth PRI can be reformulated as the measurement about the return $\mathbf{s}(\hat{t})=\mathbf{s}^r(\hat{t})|_{r=0}$ of $\boldsymbol{\beta}$ in the 0th PRI. The sparse scenario $\mathbf{s}(\hat{t})$ can be recovered using the measurement model as shown in (14) if sensing matrix $\mathbf{A}^r$ satisfies RIP.

A hardware structure having M receiver channels will be considered in the following. Owing to low SNR characteristic of returns in active radar, we resort to matching filter on the output of array $\mathbf{y}^r(\hat{t})$. The output after matching filter can be shown as

$$\mathbf{y}_{\mathrm{MF}}^r\left(\hat{t}\right)=\mathrm{MF}\left\{\mathbf{y}^r\left(\hat{t}\right)\right\}=\mathrm{MF}\left\{\mathbf{A}^r\times\mathbf{s}\left(\hat{t}\right)\right\}=\mathbf{A}^r\times\mathrm{MF}\left\{\mathbf{s}\left(\hat{t}\right)\right\}, \quad (17)$$

where $\mathrm{MF}\{\cdot\}$ denotes matching filter operation. Taking additive noise $\mathbf{n}_{\mathrm{MF}}^r(\hat{t})\in\mathbb{C}^M$ into account, the measurement model after matching filter can be expressed as

$$\mathbf{y}_{\mathrm{MF}}^r\left(\hat{t}\right)=\mathbf{A}^r\times\mathbf{s}_{\mathrm{MF}}\left(\hat{t}\right)+\mathbf{n}_{\mathrm{MF}}^r\left(\hat{t}\right), \quad (18)$$

where the return $\mathbf{s}_{\mathrm{MF}}(\hat{t})=\mathrm{MF}\{\mathbf{s}(\hat{t})\}=\mathrm{MF}\{\boldsymbol{\beta}\odot\mathbf{p}(\hat{t}-\hat{t}_T)\}$ of $\boldsymbol{\beta}$ after matching filter can be expressed as

$$\mathbf{s}_{\mathrm{MF}}\left(\hat{t}\right)=\boldsymbol{\beta}\odot\mathrm{MF}\left\{\mathbf{p}\left(\hat{t}-\hat{t}_T\right)\right\}, \quad (19)$$

where $\mathrm{MF}\{\mathbf{p}(\hat{t}-\hat{t}_T)\}$ is the output of matching filter about $\mathbf{p}(\hat{t}-\hat{t}_T)$, which is abbreviated to $\mathbf{p}^{mf}(\hat{t}-\hat{t}_T)\in\mathbb{C}^{SN}$ here. According to the expression of $\mathbf{p}(\hat{t}-\hat{t}_T)$ in (12), $\mathbf{p}^{mf}(\hat{t}-\hat{t}_T)$ can be shown as

$$\mathbf{p}^{mf}\left(\hat{t}-\hat{t}_T\right)=\left[\underbrace{(\tilde{\mathbf{p}}^{mf}(\hat{t}-\hat{t}_T))^T,\ldots,(\tilde{\mathbf{p}}^{mf}(\hat{t}-\hat{t}_T))^T}_{N}\right]^T, \quad (20)$$

where $\tilde{\mathbf{p}}^{mf}(\hat{t}-\hat{t}_T)\in\mathbb{C}^S$ is $\mathrm{MF}\{\tilde{\mathbf{p}}(\hat{t}-\hat{t}_T)\}$ as follows:

$$\begin{aligned}\tilde{\mathbf{p}}^{mf}\left(\hat{t}-\hat{t}_T\right)&=\left[\mathrm{MF}\left\{\tilde{p}_0\left(\hat{t}-\hat{t}_T\right)\right\},\ldots,\mathrm{MF}\left\{\tilde{p}_{S-1}\left(\hat{t}-\hat{t}_T\right)\right\}\right]^T\\&=\left[p_0^{mf}\left(\hat{t}-\hat{t}_T\right),\ldots,p_{S-1}^{mf}\left(\hat{t}-\hat{t}_T\right)\right]^T.\end{aligned} \quad (21)$$

Due to the sparse characteristic of $\boldsymbol{\beta}$, the return $\mathbf{s}_{\mathrm{MF}}(\hat{t})$ is also a sparse vector with the same support as $\boldsymbol{\beta}$.

Considering the return with maximum SNR after matching filter appears at the fast time $\hat{t}_{T-\mathrm{MF}}$ with respect to target at range $\hat{t}_T$, the return $\mathbf{s}_{\mathrm{MF}}(\hat{t})$ at $\hat{t}_{T-\mathrm{MF}}$ can be used as the measurement to recover the unknown sparse scenario. The version of model (18) at $\hat{t}_{T-\mathrm{MF}}$ can be shown as

$$\mathbf{y}_{\mathrm{MF}}^r=\mathbf{A}^r\times\mathbf{s}+\mathbf{n}_{\mathrm{MF}}^r, \quad (22)$$

where $\mathbf{y}_{\mathrm{MF}}^r=\mathbf{y}_{\mathrm{MF}}^r(\hat{t}_{T-\mathrm{MF}})$ and $\mathbf{n}_{\mathrm{MF}}^r=\mathbf{n}_{\mathrm{MF}}^r(\hat{t}_{T-\mathrm{MF}})$. The signal $\mathbf{s}\in\mathbb{C}^{SN}$ is the abbreviation of $\mathbf{s}_{\mathrm{MF}}(\hat{t}_{T-\mathrm{MF}})$ as follows:

$$\mathbf{s}=\mathbf{s}_{\mathrm{MF}}\left(\hat{t}_{T-\mathrm{MF}}\right)=\left[\underbrace{s_{0,0},\ldots,s_{0,S-1}}_{\text{block }0\#},\ldots,\underbrace{s_{N-1,0},\ldots,s_{N-1,S-1}}_{\text{block }N-1\#}\right]^T. \quad (23)$$

The element $s_{n,s}$, $n=0,\ldots,N-1$, $s=0,\ldots,S-1$, is the sth element in the nth block of signal $\mathbf{s}$, which can be written as $s_{n,s}=\beta_{n,s}p_s^{mf}(\hat{t}-\hat{t}_T)|_{\hat{t}=\hat{t}_{T-\mathrm{MF}}}$. Due to the same sparse characteristic between $\mathbf{s}$ and $\boldsymbol{\beta}$, the signal $\mathbf{s}$ can also be seen as target sparse scenario in the paper.

The measurement model in (22) is a SMV model in CS framework; sparse scenario $\mathbf{s}$ could be reconstructed via the solution as shown in (1) when the number of measurements M is sufficient and SNR is sufficiently high. During an observation period, the R measurements $\{\mathbf{y}_{\mathrm{MF}}^{r}\}_{r=0}^{R-1}$ at the same fast time $\widehat{t}_{T-\mathrm{MF}}$ in R pulse repetition intervals satisfy MMV measurement model and then can be used to recover sparse target scenario $\mathbf{s}$ through MUSIC, SOMP [7], and CS-MUSIC [14]. What should be highlighted is that the model in (22) is developed based on multireceiver structure which needs the same number of receivers as receiving array sensors. This multireceiver structure is more expensive in price and larger in volume than traditional receiver structure in active radar. In the next section, the proposed strategy which employs multisensor single-receiver structure is presented to recover the sparse target scenario.

2.2. Measurement Model Using Single-Receiver. According to (14), there are R measurements about a fixed return $\mathbf{s}(\widehat{t})$ with respect to target scenario $\boldsymbol{\beta}$ at the same fast time $\widehat{t}$ during an observation period. In CS framework, few measurements about a sparse signal using random waveforms can be used to recover the original sparse signal with overwhelming probability. Inspired by this mechanism, the outputs of M subarray $\mathbf{y}^{r}(\widehat{t})$ can be randomly weighted through M phase shifters and then be summarized using single-receiver channel. The random weighted and summarized version of $\mathbf{y}^{r}(\widehat{t})$ is shown as follows:

$$z^{r}(\widehat{t}) = \left(\mathbf{f}^{r}\right)^{T}\mathbf{A}^{r}\mathbf{s}(\widehat{t}), \quad r = 0,\ldots,R-1, \tag{24}$$

where $\mathbf{f}^{r} = [\phi_{0}^{r},\ldots,\phi_{M-1}^{r}]^{T} \in \mathbb{C}^{M}$, $r = 0,\ldots,R-1$, is the random weight in rth PRI. The weights remain unchanged in a pulse repetition period but take different values in different period. The element ϕ_{m}^{r} in $\mathbf{f}^{r}$ may be a random Bernoulli variable; for example, $\phi_{m}^{r} = \{\pm 1, \text{w.p. } 1/2\}$, $m = 0,\ldots,M-1$.

In principle, the random weighing onto $\mathbf{y}^{r}(\widehat{t})$ should be put into practice using M additional phase shifters connecting to the outputs of M subarrays. Assuming that B array elements belonging to mth subarray, $m = 0,\ldots,M-1$, can form the beam pointing to Ω when phase shifters of B corresponding transmitter and receiver (T/R) modules are set up as $C_{m}' = \{C_{m,b}'\}_{b=0}^{B-1}$ during the reception, the random weighting procedure as shown in (24) can be accomplished if phased shifters of T/R modules change their setup as $C_{m}'' = \phi_{m}^{r}C_{m}' = \{\phi_{m}^{r}C_{m,b}'\}_{b=0}^{B-1}$. Accordingly, there is no requirement of additional phase shifters to achieve the random weighting onto the outputs of equivalent sensors.

According to (24), the measuring model with respect to the fixed return $\mathbf{s}(\widehat{t})$ of target scenario $\boldsymbol{\beta}$ can be formulated as

$$\begin{bmatrix} z^{0}(\widehat{t}) \\ \vdots \\ z^{R-1}(\widehat{t}) \end{bmatrix} = \begin{bmatrix} \left(\mathbf{f}^{0}\right)^{T} \times \mathbf{A}^{0} \\ \vdots \\ \left(\mathbf{f}^{R-1}\right)^{T} \times \mathbf{A}^{R-1} \end{bmatrix} \times \mathbf{s}(\widehat{t}). \tag{25}$$

The above model can be rewritten as

$$\mathbf{z}(\widehat{t}) = \boldsymbol{\Phi} \times \mathbf{A}^{s} \times \mathbf{s}(\widehat{t}), \tag{26}$$

where $\mathbf{z}(\widehat{t}) = [z^{0}(\widehat{t}),\ldots,z^{R-1}(\widehat{t})]^{T}$ is the measurements about $\mathbf{s}(\widehat{t})$ through random weighting, and $\boldsymbol{\Phi} \in \mathbb{C}^{R\times RM}$ is the measurement matrix with block-diagonal structure as follows:

$$\begin{aligned} \boldsymbol{\Phi} &= \operatorname{diag}\left(\left(\mathbf{f}^{0}\right)^{T},\ldots,\left(\mathbf{f}^{R-1}\right)^{T}\right) \\ &= \begin{bmatrix} \left(\mathbf{f}^{0}\right)^{T} & & \mathbf{0} \\ & \ddots & \\ \mathbf{0} & & \left(\mathbf{f}^{R-1}\right)^{T} \end{bmatrix}. \end{aligned} \tag{27}$$

The matrix $\mathbf{A}^{s} \in \mathbb{C}^{RM\times SN}$ is a joint angle-Doppler representation basis, which is a stack of R matrices as follows:

$$\mathbf{A}^{s} = \left[\left(\mathbf{A}^{0}\right)^{T},\ldots,\left(\mathbf{A}^{R-1}\right)^{T}\right]^{T} = \begin{bmatrix} \mathbf{A}^{0} \\ \vdots \\ \mathbf{A}^{R-1} \end{bmatrix}, \tag{28}$$

where the element $\mathbf{A}^{r}$, $r = 0,\ldots,R-1$, is shown as (16).

The summarization after random weighing as shown in (24) should also be processed via matching filter to improve SNR. Substituting (15), (16), and (19) into (24), a version of $z^{r}(\widehat{t})$ after matching filter can be expressed as follows:

$$\begin{aligned} & z_{\mathrm{MF}}^{r}(\widehat{t}) \\ &= \mathrm{MF}\{z^{r}(\widehat{t})\} \\ &= \mathrm{MF}\Bigg\{\Bigg[\underbrace{e^{j2\pi f_{0}^{d}t_{r}}\left(\mathbf{f}^{r}\right)^{T}\times\mathbf{a}_{0},\ldots,e^{j2\pi f_{S-1}^{d}t_{r}}\left(\mathbf{f}^{r}\right)^{T}\times\mathbf{a}_{0}}_{\text{block } 0\#},\ldots, \\ &\qquad \underbrace{e^{j2\pi f_{0}^{d}t_{r}}\left(\mathbf{f}^{r}\right)^{T}\times\mathbf{a}_{N-1},\ldots,e^{j2\pi f_{S-1}^{d}t_{r}}\left(\mathbf{f}^{r}\right)^{T}\times\mathbf{a}_{N-1}}_{\text{block } N-1\#}\Bigg] \\ &\qquad \times \mathbf{s}(t)\Bigg\} \\ &= \sum_{n=0}^{N-1}\sum_{s=0}^{S-1}\left\{e^{j2\pi f_{s}^{d}t_{r}}\left(\mathbf{f}^{r}\right)^{T}\times\mathbf{a}_{n}\right\}\cdot\mathrm{MF}\{s_{n,s}(\widehat{t})\} \\ &= \left(\left(\mathbf{f}^{r}\right)^{T}\times\mathbf{A}^{r}\right)\times\mathbf{s}_{\mathrm{MF}}(\widehat{t}), \quad r = 0,\ldots,R-1. \end{aligned} \tag{29}$$

The measuring model corresponding to (26) after matching filter can be obtained based on (29) as follows:

$$\mathbf{z}_{\mathrm{MF}}(\widehat{t}) = \boldsymbol{\Phi}\times\mathbf{A}^{s}\times s_{\mathrm{MF}}(\widehat{t}) + \mathbf{n}_{\mathrm{MF}}(\widehat{t}), \tag{30}$$

where $\mathbf{n}_{\mathrm{MF}}(\widehat{t}) \in \mathbb{C}^{R}$ is the additive noise of measurement and $\mathbf{z}_{\mathrm{MF}}(\widehat{t}) = \mathrm{MF}\{\mathbf{z}(\widehat{t})\}$ can be expressed as $[z_{\mathrm{MF}}^{0}(\widehat{t}),\ldots,z_{\mathrm{MF}}^{R-1}(\widehat{t})]^{T}$ which is a R-dimension measurement.

As described above, the measurement at $\widehat{t}_{T-\mathrm{MF}}$ of $\mathbf{z}_{\mathrm{MF}}(\widehat{t})$ where the return after matching filter has maximum SNR can be shown as

$$\mathbf{z} = \boldsymbol{\Phi}\times\mathbf{A}^{s}\times\mathbf{s} + \mathbf{n}, \tag{31}$$

where $\mathbf{z} = \mathbf{z}_{\mathrm{MF}}(\widehat{t}_{T-\mathrm{MF}})$; $\mathbf{s} = \mathbf{s}_{\mathrm{MF}}(\widehat{t}_{T-\mathrm{MF}})$ is expressed in (23) which can be seen as sparse target scenario; $\mathbf{n} = \mathbf{n}_{MF}(\widehat{t}_{T-\mathrm{MF}})$

is additive Gaussian noise and $\mathrm{Re}(\mathbf{n}),\ \mathrm{Im}(\mathbf{n}) \sim N(0,\sigma^2\mathbf{I}_R)$, where $\mathrm{Re}(\mathbf{n})$ and $\mathrm{Im}(\mathbf{n})$ denote real and imaginary parts, respectively; $\mathbf{I}_R$ denotes R-dimension identity matrix. For the convenience of analysis, $\mathbf{D} = \mathbf{\Phi}\mathbf{A}^s$ is denoted as equivalent dictionary, and then (31) can be rewritten as

$$\mathbf{z} = \mathbf{D} \times \mathbf{s} + \mathbf{n}. \tag{32}$$

Dictionary $\mathbf{D}$ can be expressed as

$$\mathbf{D} = \left[\underbrace{\mathbf{d}_{0,0},\ldots,\mathbf{d}_{0,S-1}}_{\text{block } 0\#},\ldots,\underbrace{\mathbf{d}_{N-1,0},\ldots,\mathbf{d}_{N-1,S-1}}_{\text{block } N-1\#}\right], \tag{33}$$

where $\mathbf{d}_{n,s}, n = 0,\ldots,N-1;\ s = 0,\ldots,S-1$, denotes the s-column in nth block of $\mathbf{D}$. The SNR of the return $s_{n,s} \in \mathbf{s}$ after matching filter about target $\beta_{n,s} \in \boldsymbol{\beta}$ is defined as

$$\mathrm{SNR}_{n,s} = \frac{\left|s_{n,s}\right|^2 \cdot \left\|\mathbf{d}_{n,s}\right\|_2^2}{R \cdot \left(2\sigma^2\right)}, \tag{34}$$

where $n = 0,\ldots,N-1,\ s = 0,\ldots,S-1$.

As shown in (31), we develop a measurement model with respect to sparse target scenario $\mathbf{s}$ (equivalent to $\boldsymbol{\beta}$) using a joint angle-Doppler representation, which needs only one receiver channel. The measurement is an SMV model in CS framework in which the equivalent dictionary $\mathbf{D}$ satisfies RIP when the number of measurement R is sufficient; therefore, the estimated target scenario $\widehat{\mathbf{s}} \in \mathbb{C}^{SN}$ can be recovered via the solution as shown in (1). The reconstructed $\widehat{\mathbf{s}}$ can be rewritten as $\widehat{\mathbf{s}} = [\widehat{\mathbf{s}}_0^T,\ldots,\widehat{\mathbf{s}}_{N-1}^T]^T$ in which element $\widehat{\mathbf{s}}_n = [\widehat{s}_{n,0},\ldots,\widehat{s}_{n,S-1}]^T,\ n = 1,\ldots,N-1$ denotes the amplitude vector on the Doppler dictionary F of target located in the nth spatial grid of Ω. Integrating energies distributed in all Doppler elements on F for every nth target in Ω, a recovered target scenario defined on Ω can be shown as follows:

$$\widehat{\mathbf{s}}_\Omega = \left[\left\|\widehat{\mathbf{s}}_0\right\|_2,\ldots,\left\|\widehat{\mathbf{s}}_{N-1}\right\|_2\right]^T. \tag{35}$$

3. Sparse Target Scenario Recovery

In Section 2, the Doppler dictionary F is assumed as a known set during the generation of $\mathbf{A}^r$; in the practice, F is unknown because relative velocities between targets and radar are not priori. In this section, F is built using radar returns and then matrices $\mathbf{A}^r$ and $\mathbf{A}^s$ are presented; in the end, target scenario can be recovered based on measurement model (31).

3.1. Estimation of Targets' Doppler. A PAR should work on a conventional mode with one illumination and one receiving beam via appropriate setup on phase shifters. The radar returns including R' pulse in one observation period with respect to K targets distributed in Ω; at the same range, $\widehat{t}_T$ can be expressed as follows:

$$q^r\left(\widehat{t}\right) = \sum_{k=0}^{K-1} \beta_k p\left(\widehat{t} - \widehat{t}_T\right) \exp\left[j2\pi x_k\left(\widehat{t} + t_r\right)\right], \quad r = 0,\ldots,R'-1, \tag{36}$$

where $X = \{x_k, k = 0,\ldots,K-1\}$ denotes the actual targets' Doppler set and $\beta_k,\ k = 0,\ldots,K-1$ denotes the kth target amplitude. The outputs after matching filter about the return in (36) at the same fast time $\widehat{t} = \widehat{t}_{T-\mathrm{MF}}$ where maximum SNR level exists are

$$q^r = \sum_{k=0}^{K-1} \beta_k^{mf} \exp\left(j2\pi x_k t_r\right), \quad r = 0,\ldots,R'-1, \tag{37}$$

where $\beta_k^{mf},\ k = 0,\ldots,K-1$, is the corresponding target amplitude after matching filter. According to (37), the returns at the same fast time $\widehat{t}_{T-\mathrm{MF}}$ during R' pulse repetition periods are linear combination of K complex sinusoids on the slow time dimension.

Due to the sparse consideration about target scenario, the number of complex sinusoids in (37) is far less than the number of the frequencies in set F_B which contains all possible Doppler frequencies in radar returns when the pulse repetition frequency is $F_r = 1/T_r$. The set F_B stems from discretizing $[0, F_r]$ with an interval Δf as follows:

$$F_B = \left\{f_b = b \cdot \Delta f, b = 0,\ldots,B-1\right\}, \tag{38}$$

where $B = F_r/\Delta f, B \gg K$. In consequence, X could be reconstructed using CS framework. A sparse target scenario $\boldsymbol{\alpha} \in \mathbb{C}^B$ defined on F_B can be expressed as

$$\boldsymbol{\alpha} = \left[\alpha_0,\ldots,\alpha_{B-1}\right]^T, \tag{39}$$

where $\alpha_b = \beta_k^{mf}$ when $f_b = x_k$; otherwise $\alpha_b = 0$ for $b = 0,\ldots,B-1$ and $k = 0,\ldots,K-1$. Consequently, there are K nonzero elements in $\boldsymbol{\alpha}$. The returns as shown in (37) can be reformulated as

$$\mathbf{q} = \mathbf{E}\boldsymbol{\alpha} + \mathbf{n}, \tag{40}$$

where $\mathbf{q} = [q^0,\ldots,q^{R'-1}]^T \in \mathbb{C}^{R'}$ is the measurement; $\mathbf{n} \in \mathbb{C}^{R'}$ is additive noise; and $\mathbf{E} \in \mathbb{C}^{R'\times B}$ is the representation basis in frequency domain as follows:

$$\mathbf{E} = \left[\mathbf{e}(0),\ldots,\mathbf{e}(B-1)\right]. \tag{41}$$

The column $\mathbf{e}(b) \in \mathbb{C}^{R'},\ b = 0,\ldots,B-1$, of $\mathbf{E}$ can be shown as

$$\mathbf{e}(b) = \left[\exp\left(j2\pi f_b t_0\right),\ldots,\exp\left(j2\pi f_b t_{R'-1}\right)\right]^T, \tag{42}$$

where $f_b = b \cdot \Delta f$ and $t_r = r \cdot T_r,\ r = 0,\ldots,R'-1$.

Considering measurement model (40), measuring matrix $\mathbf{E}$ is a redundant dictionary in frequency domain. The sparse signal $\boldsymbol{\alpha}$ can be recovered using $R' \ll B$ measurements in CS framework [17]. Denoting $\widehat{\boldsymbol{\alpha}} = [\widehat{\alpha}_0, \ldots, \widehat{\alpha}_{B-1}]$ as the reconstructed signal, the estimated targets' Doppler set can be obtained when we detect signals in $\widehat{\boldsymbol{\alpha}}$ through an appropriate threshold T_h. Assuming that the signal indices in $\widehat{\boldsymbol{\alpha}}$ where the magnitude is larger than T_h is $\Omega_b = \{b \mid |\widehat{\alpha}_b| \geq T_h, b = 0, \ldots, B-1\}$, then the estimated target Doppler $\widehat{X}$ can be shown as follows if we rewrite Ω_b as $\Omega_b = \{b(k), k = 0, \ldots, \widehat{K}-1\}$:

$$\widehat{\mathrm{X}} = \left\{ f_{b(k)} = b(k)\,\Delta f, b(k) \in \Omega_b \right\}, \tag{43}$$

where $\widehat{K}$ is the element number of Ω_b.

3.2. Generation of Doppler Dictionary. In Section 3.1, an estimated targets' Doppler set $\widehat{X}$ defined on discretized set F_B is presented. In general, the actual target Doppler $x_k \in X$ does not accurately lie on the grid of F_B; hence, x_k can be expressed as $x_k = b(k)\Delta f + \Delta x_k$ where $|\Delta x_k| \leq 0.5\Delta f$ is the error between x_k and its approximating frequency $b(k)\Delta f, b(k) \in \Omega_b$ in F_B. When the error term Δx_k is large enough, more than one frequency components will appear in $\widehat{X}$ to approximate actual Doppler x_k. For example, if the error $\Delta x_k = 0.5\Delta f$, that is, $x_k = b(k) \cdot \Delta f + 0.5\Delta f$, two frequencies $b(k)\Delta f$ and $(b(k)+1)\Delta f$ whose magnitude exceed detection threshold may arise in $\widehat{X}$. In conclusion, there are usually more frequency components in the estimated Doppler set $\widehat{X}$ than actual set X, that is, $\widehat{K} \geq K$.

With respect the measurement model (31), sparse scenario $\boldsymbol{\beta}$ could be recovered with overwhelming probability when the number of measurement $R \geq C\mu^2(\boldsymbol{\Phi}, \mathbf{A}^s)K\log(SN)$ [2], where $\mu(\boldsymbol{\Phi}, \mathbf{A}^s)$ is the mutual coherence between $\boldsymbol{\Phi}$ and $\mathbf{A}^s$. Therefore, while R and N are fixed; then, the number of frequencies in dictionary F must satisfy $S \leq S_{\max}$ where $S_{\max}$ denotes the maximum numerical value which assure that the measurement matrix in (31) satisfy RIP. In summary, the frequency number in dictionary F should satisfy $\widehat{K} \leq S \leq S_{\max}$. The Doppler dictionary F can be generated based on $\widehat{X}$ in order to include all possible components in actual Doppler set X. Generally, F may be formulated as

$$F = \widehat{X}. \tag{44}$$

In the case where the component number of $\widehat{X}$ is small, we can appropriately extend dictionary F based on $\widehat{X}$. For example, there is a neighbor frequency whose amplitude is close to but not larger than detection threshold T_h, so we can put this neighbor frequency into $\widehat{X}$ in order that dictionary F includes all actual Doppler in X as far as possible.

3.3. Resolution of Doppler Dictionary. The Doppler dictionary F which is employed to produce joint angle-Doppler representation $\mathbf{A}^s$ comes from the estimated targets' Doppler set $\widehat{X}$ in which the frequency resolution depends on the resolution of F_B; therefore the resolution of F is Δf. As expressed in (28), the representation basis $\mathbf{A}^s$ is the stack of multiple $\mathbf{A}^r$. The $S \cdot N$ columns in $\mathbf{A}^s$ can be divided into N blocks in which each one comprises S subcolumns. According to (16) and (28), the (n, s)th column $\mathbf{a}^s_{n,s} \in \mathbb{C}^{SN}$ in $\mathbf{A}^s\,\forall n \in [0, N-1],\ s \in [0, S-1]$, which denotes the sth subcolumn of nth block, can be expressed as follows:

$$\mathbf{a}^s_{n,s} = \left[\exp\left(j2\pi f_s t_0\right)\mathbf{a}^T_n, \ldots, \exp\left(j2\pi f_s t_{R-1}\right)\mathbf{a}^T_n\right]^T. \tag{45}$$

In $\mathbf{a}^s_{n,s}$, the identical items $\mathbf{a}_n$ models for the relationship of spatial phases embedded in the M subarrays output due to a target located in $\mathbf{u}_n \in \Omega$ in spatial domain, and the items $\exp(j2\pi f_s t_r),\ r = 0, \ldots, R-1$, models for phase relationship existing in returns of all subarrays due to a target having Doppler $f_s \in F$ on the slow time dimension.

As addressed above, there usually is an estimating error Δx_k between actual Doppler x_k and its estimation $f_s = b(k)\Delta f \in F$ as shown in $x_k = b(k)\Delta f + \Delta x_k$. During an observation period including R pulses, the actual phase history in the slow time domain is $\{\exp(j2\pi x_k t_r), r = 0, \ldots, R-1\}$, while the phase history in the column $\mathbf{a}^s_{n,s}$ corresponding to sth components $f_s \in F$ is $\{\exp(j2\pi f_s t_r), r = 0, \ldots, R-1\}$. The phase error ΔP between the above two phase histories is $\Delta P = 2\pi \cdot \Delta x_k \cdot (t_{R-1} - t_0)$. In order to reduce the loss due to the phase error ΔP, we impose a limit $\Delta P < \pi/4$ for all possible estimating errors Δx_k. Considering the maximum value of $\Delta x_k = 0.5\Delta f$, the resolution Δf in F should satisfy

$$\Delta f < \frac{1/4}{t_{R-1} - t_0}, \tag{46}$$

where $(t_{R-1} - t_0) = R \cdot T_r$ is the time of duration during in an observation period as shown in model (31).

3.4. The Choice on the Measurement Number. In CS framework, more measurements can bring better recovery performance; therefore, the measurement number R in model (31) should be as large as possible. As described above, R is the number of pulses during a radar observation, so there are 3 factors about R being taken into account in the practice. Firstly, because the maximum moving distance between the radar platform and targets should not be longer than a radar range cell during an observation, so the choice of R should satisfy inequality $v_{\max} \cdot (RT_r) \leq r_{\text{cell}}$ where $v_{\max}$ denotes the maximum relative velocity between radar and targets and r_{cell} denotes the range cell of radar. Secondly, the increment of measurement number R brings more computational complexity in the procedure of CS recovery; therefore, the value of R should not be too large in order that the digital signal processor (DSP) of the radar can meet the computational demand. In general, the choice of R should assure that CS recovery can be finished in one observation period. Lastly, the measurement number R must satisfy (46); that is, $R < (1/4)/(\Delta f \cdot T_r)$, which assures that the phase error ΔP between the actual and the represented phase history cannot be more than $\pi/4$. In summary, the value of R should be as large as possible after the consideration on the above 3 factors.

For example, if the range cell of radar is $r_{\text{cell}} = 5$ m, the PRI is $T_r = 100\,\mu$s, and the maximum relative velocity between

radar and targets is $v_{\max} = 100\,\mathrm{m/s}$; the measurement number needs to satisfy $R \le r_{\mathrm{cell}}/(v_{\max} \cdot T_r) = 500$ according to the first factor in the above. If the resolution of Doppler dictionary F is set as $\Delta f = 25\,\mathrm{Hz}$, the measurement number should satisfy $R < (1/4)/(\Delta f \cdot T_r) = 100$ based on the factor 3. Supposing that the computation power of the DSP of radar is sufficient to accomplish the recovery procedure, the choice on the measurement number should satisfy $R < 100$ after consideration on the factor 1 and the factor 3.

3.5. Sparse Target Scenario Reconstruction. Based on the above description, we could reconstruct the sparse target scenario through the procedure as follows.

(1) Select the appropriate resolution of F according to (46) and then build the discretized frequency set F_B in (38).

(2) Setup radar on the mode of one illumination and one receiving beam. Get the estimated Doppler set $\widehat{X}$ in (43) from the measurement model in (40).

(3) Produce the Doppler dictionary F according to (44).

(4) Setup radar on the mode of multisensor single-receiver. Get the recovered $\widehat{\mathbf{s}}$ according to measurement model (31) and then the target scenario $\widehat{\mathbf{s}}_\Omega$ in Ω from (35).

The toolbox CVX [18] is employed to reconstruct $\boldsymbol{\alpha}$ in measurement model (40) and $\mathbf{s}$ in (31) according to the solution as shown in (1).

4. Numerical Experiments

In the section, the performance of the proposed strategy is evaluated through numerical experiments and the algorithm MUSIC is employed as a benchmark for comparison. What should be noted is that the proposed strategy as shown in (31) needs only one receiver channel, while the MUSIC algorithm is based on the measuring model as shown in (22) which needs multiple receiver channels. That is, the proposed strategy takes a more economical way than the benchmark algorithm MUSIC on the measurement about target scenario.

A PAR with wavelength $\lambda = 0.02\,\mathrm{m}$ is considered in all experiments. The shape of array plane is a circle with diameter 12.5λ, and all array sensors are partitioned into $M = 8$ subarrays which are randomly distributed in the array plane. The interest target area $\Omega = \{|\theta| \le 3^\circ, \varphi \in [0, 2\pi]\}$ is uniformly discretized into $N = 37$ grids. The radar PRI is $100\,\mu\mathrm{s}$, the range cell of radar is set as $r_{\mathrm{cell}} = 5\,\mathrm{m}$, and the relative velocity between radar and targets is not more than $v_{\max} = 100\,\mathrm{m/s}$. An experiment point $\mathrm{St} = \{K, \mathrm{SNR}\}$ is defined when target numbers K and SNRare fixed. With respect to each point St, 1000 times of independent numerical experiments are executed to evaluate the recovery performance.

4.1. The Procedure of One Experiment. The procedure of one numerical experiment will be illustrated using an example. In the example, a sparse target scenario where two adjacent targets are randomly distributed in Ω is investigated. The SNRs of two targets are both equal to 3 dB, and their Doppler sets are 3765 Hz and 3870 Hz, respectively. The procedure of the proposed strategy is shown as follows.

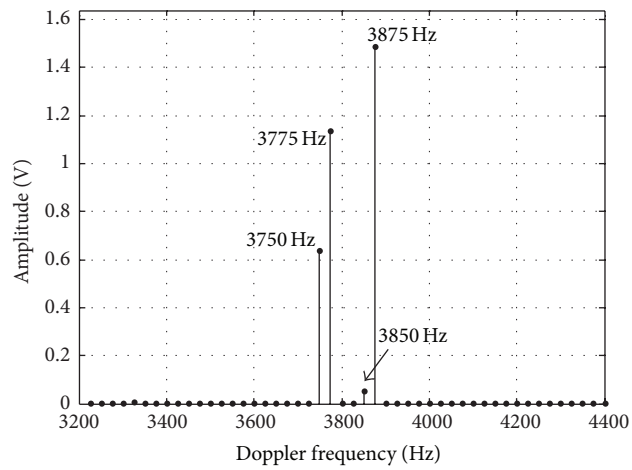

Figure 3: Recovered target scenario $\widehat{\boldsymbol{\alpha}}$ in Doppler domain.

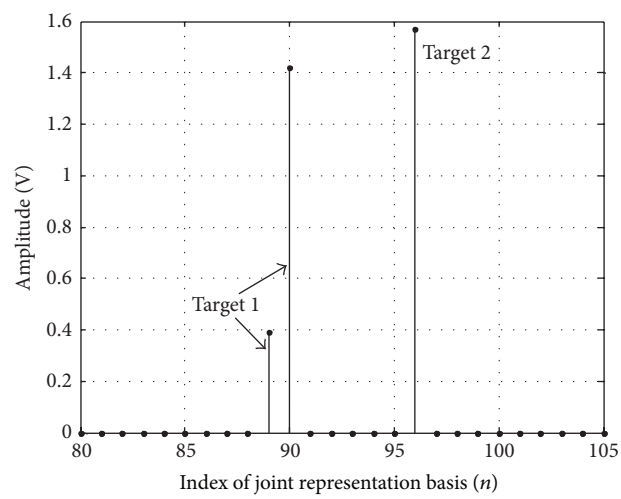

Figure 4: Recovered target scenario $\widehat{\mathbf{s}}$ in joint angle-Doppler domain.

(1) Firstly, the number of measurements in model (31) is set up as $R = 80$ which will not bring the migration across a range cell r_{cell} during a radar observation period as illustrated in Section 3.4, so, according to (46), the resolution of dictionary F should satisfy $\Delta f < 0.25/(RT_r)$; that is, $\Delta f < 31\,\mathrm{Hz}$. In the experiment, the resolution Δf is set to 25 Hz. (2) According to model (37), sparse target scenario $\widehat{\boldsymbol{\alpha}}$ in Doppler domain is achieved using $R' = 100$ returns. The signal $\widehat{\boldsymbol{\alpha}}$ is a B-dimension vector where $B = F_r/\Delta f = 400$ and one part of it is depicted as Figure 3.

As shown in Figure 3, the estimated Doppler set $\widehat{X}$ is $\{3750, 3775, 3875\}\mathrm{Hz}$ after detection. There are 3 numbers of elements in $\widehat{X}$ which are larger than the real number of targets; that is, $(|\widehat{X}| = 3) > (K = 2)$ because actual target Doppler $\{x_1, x_2\}$ does not accurately lie on the

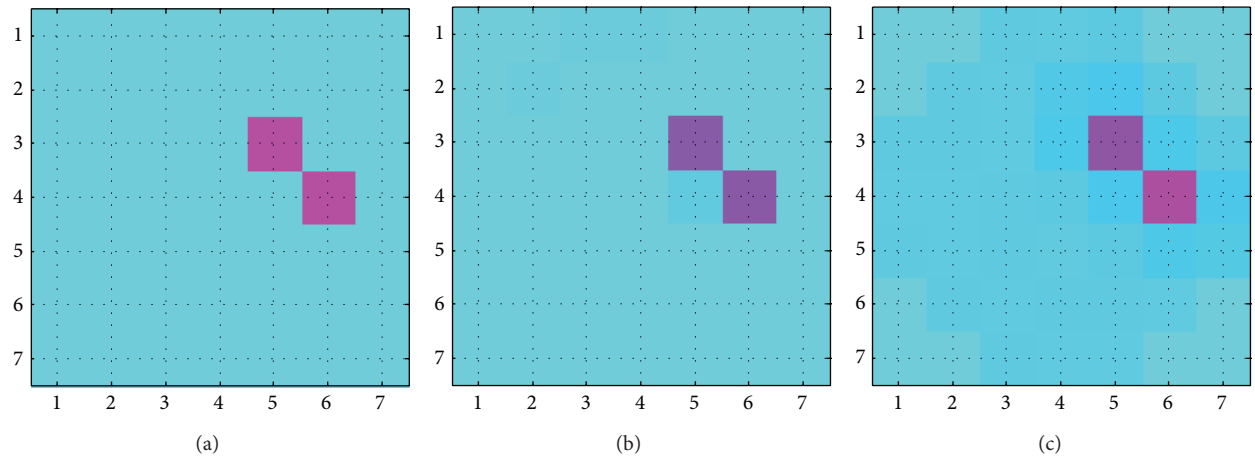

Figure 5: Recovered target scenario with two adjacent targets. (a) Original target scenario. (b) Recovery of the proposed strategy. (c) Recovery of MUSIC.

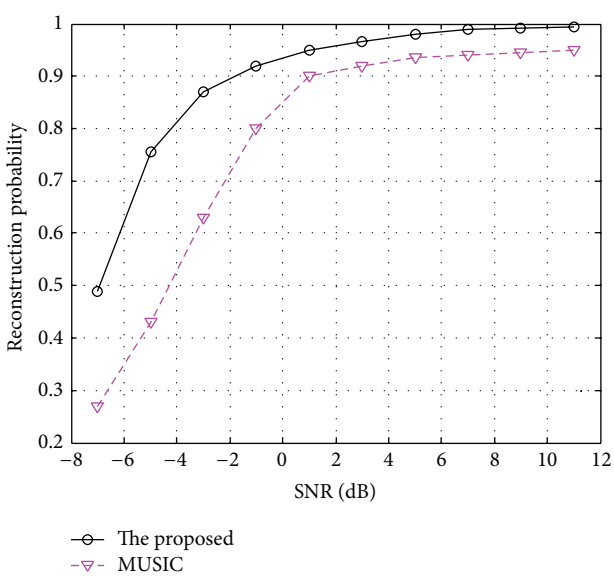

Figure 6: Reconstruction probability with two adjacent targets.

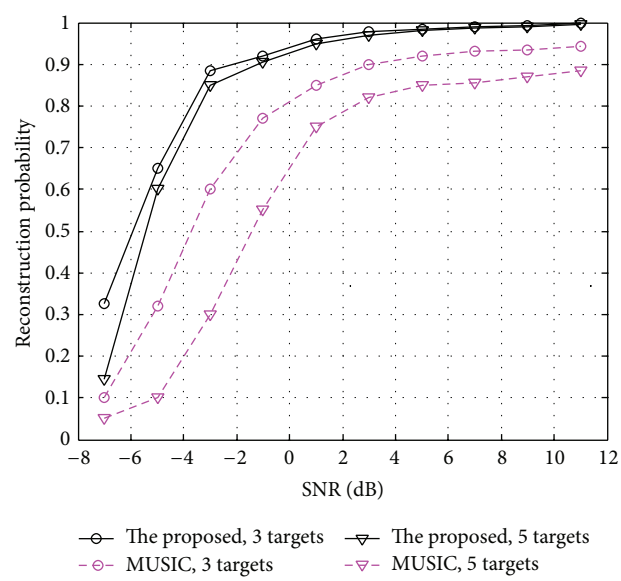

Figure 7: Reconstruction probability with multiple randomly distributed targets.

grid of discretized Doppler set F_B, where $|\cdot|$ denotes the element number of set. (3) Because a frequency leakage arises in 3850 Hz around a large component 3875 Hz and the estimated target number $|\widehat{X}|$ is not large, we put 3850 Hz in dictionary F. So the used F is $\widehat{X} \cup \{3850\}$; that is, $F = \{3750, 3775, 3850, 3875\}$ in this step, and then the element number of F is $S = |F| = 4$. (4) The sparse scenario $\widehat{\mathbf{s}}$ represented in joint angle-Doppler domain is reconstructed from model (31) as shown in Figure 4. In the figure, the horizontal axis n is the grid index of joint angle-Doppler domain. An arbitrary nth grid in the horizontal axis can be written as $n = (p-1) \cdot S + q$, where $p \in [1, N]$ denotes the pth spatial grid of discretized Ω and $q \in [1, S]$ denotes qth frequency of dictionary F.

As depicted in Figure 4, target 1 occupies two grids in joint angle-Doppler domain; that is, the energy of target 1 spreads into two frequencies in dictionary F because we use a representation on discretized set F_B to approximate an actual Doppler defined in a continuous frequency domain. According to $\widehat{\mathbf{s}}$, the sparse scenario $\widehat{\mathbf{s}}_\Omega$ defined in spatial domain Ω can be obtained from (35) as shown in Figure 5.

In Figure 5, the horizontal axis is the index of discretized azimuth and vertical axis corresponds to discretized elevation in Ω. It is seen that the performance of the proposed strategy is better than traditional MUSIC with less and lower sidelobes around actual targets.

4.2. Resolution of Two Adjacent Targets. With respect the scenario of two adjacent targets in Ω at the same range cell for active radar, the performance of the proposed strategy is investigated in different SNRs. In each experiment, two

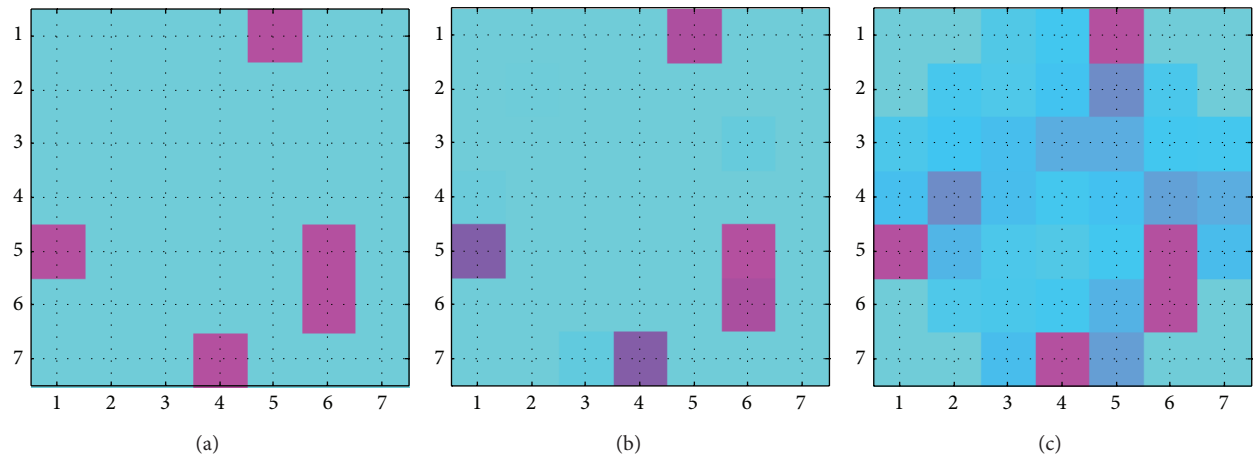

FIGURE 8: Recovered target scenario with 5 randomly distributed targets. (a) Original Scenario. (b) Recovery of the proposed strategy. (c) Recovery of MUSIC.

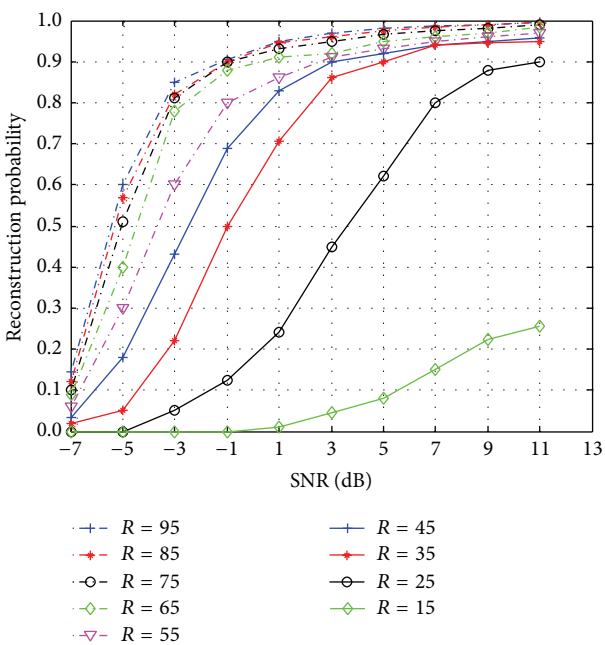

FIGURE 9: Reconstruction probability of the proposed strategy when $K = 5$.

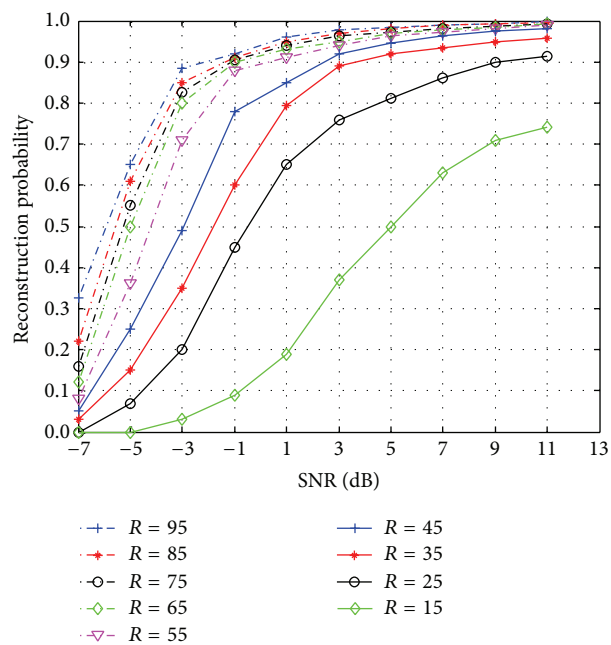

FIGURE 10: Reconstruction probability of the proposed strategy when $K = 3$.

adjacent angles are randomly selected from Ω. As shown in Figure 6, the reconstruction probability of the proposed strategy is improved with the increase of SNR and is larger than MUSIC algorithm. The proposed strategy achieves more than 90% successful recovery probability when the SNR is larger than -1 dB. According to the result of this subsection, the proposed strategy can determine the target scenarios including two adjacent targets randomly distributed in the spatial domain Ω in the forward-looking direction.

4.3. Resolution of Multiple Randomly-Distributed Targets. In this subsection, the performance of the proposed strategy with respect to the sparse scenario where multiple targets are randomly distributed in Ω is evaluated. In each experiment, the measurement number R in model (31) is equal to 96 and R' in model (40) is 100. As shown in Figure 7, the proposed approach shows better performance than MUSIC, especially at lower SNR level. The performance of the proposed strategy is almost not influenced by the number of targets whereas the performance of MUSIC obviously decays along with the increasing number of targets.

Figure 8 shows the recovered target scenario of one numerical experiment when the experiment point is $\mathrm{St} = \{5, 1\}$. As illustrated in Figure 8, there are less and lower sidelobes around actual targets in the reconstructed scenario of the proposed strategy than MUSIC algorithm.

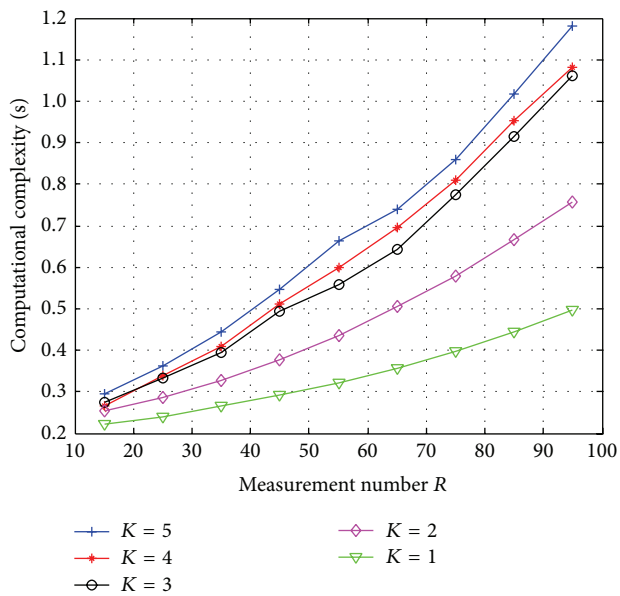

Figure 11: Computational complexity of the proposed strategy.

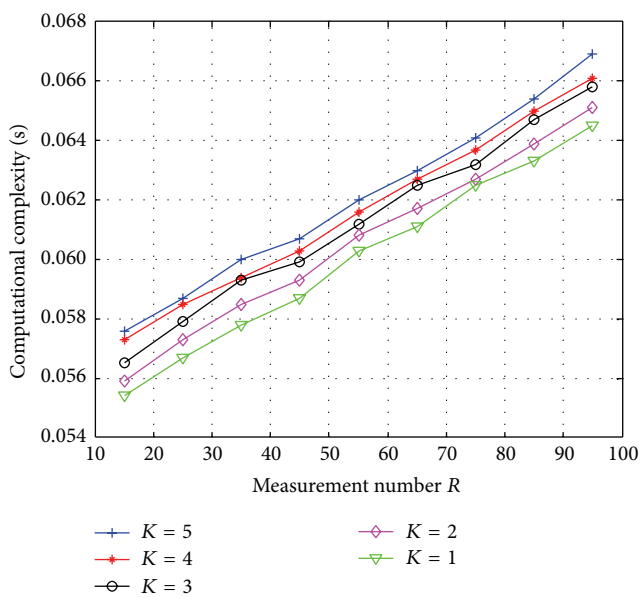

Figure 12: Computational complexity of the MUSIC algorithm.

According to the results in this subsection, the proposed strategy can determine the sparse scenario containing multiple randomly distributed targets in the spatial domain Ω in the forward-looking direction for active radar.

4.4. The Influence of Measurement Number. In the subsection, the reconstruction probability of the proposed strategy along with different measurement number R is investigated. Figure 9 shows the performance of the proposed strategy when target number $K = 5$. As depicted in Figure 9, there is little difference among the reconstructed probabilities when R takes large values, for example, $R \in [65, 95]$, but the difference becomes remarkable when R takes small values, for example, $R \in [15, 35]$. The dramatic increment of the recovery probability is the common characteristic of CS recovery procedure when the measurement number R takes small value. The recovery performance when target number $K = 3$ is depicted in Figure 10. As shown in Figure 10, the recovery probability when $K = 3$ is subject to similar characteristic as $K = 5$.

According to Figures 9 and 10, the recovery probability may be almost changeless when the measurement number R takes the values which are larger than a threshold R_{th}; for example, R_{th} may be equal to 65 when $K = 5$ and may be equal to 55 when $K = 3$. In nature, R_{th} can be seen as the smallest value which meets the condition $R \geq C\mu^2(\mathbf{\Phi}, \mathbf{A}^s)K\log(SN)$, which can assure that the equivalent dictionary $\mathbf{D} = \mathbf{\Phi}\mathbf{A}^s$ satisfies RIP in CS framework. According to Figures 9 and 10, the recovery probability of the proposed strategy can reach a desirable level if the SNR is sufficiently high although the measurement number R take a lower value. For example, the reconstruction probability will be more than 90% when SNR ≥ 3 if the measurement number $R \geq 45$ as shown in Figure 10.

4.5. Computational Complexity. In this subsection, the computational complexity of the proposed approach is addressed through numerical experiments. In the numerical experiments, the measurement number R in model (31) varies from 15 to 95 to evaluate the computational cost with respect to target number $K \in [1, 5]$. The hardware platform to carry out the experiments is "Intel Core 2 Duo CPU E7400 at 2.80 GHz, 3G Memory," and the software is "Matlab R2011a." The computational complexity of the proposed strategy is depicted in Figure 11.

As shown in Figure 11, the computational cost of the proposed strategy becomes more expensive when the target number K and the measurement number R become larger, and the cost slope becomes larger along with the increment of measurement number R and target number K.

As shown in Figure 12, the computational cost of the MUSIC algorithm slightly increases with the measurement number R and the target number K. According to Figures 11 and 12, the computation cost of the proposed strategy is more expensive than the MUSIC algorithm. The difference of the computational complexity between the proposed strategy and MUSIC algorithm becomes more obvious while the measurement number R becomes larger. The running time of the proposed strategy is approximately 17 times more than MUSIC when $R = 95$ and $K = 5$, however, 4 times when $R = 15$ and $K = 1$. Consequently, the computational complexity should be paid more attention when the measurement number R takes large values in the proposed strategy.

5. Conclusions

Based on compressive sensing framework, a strategy using joint angle-Doppler representation basis is proposed which can determine a sparse target scenario in spatial domain

at the same range for active radar in the forward-looking direction. The proposed approach does settle the trouble that traditional SAR and DBS techniques cannot provide an image for active radar in the line of sight and needs only single-receiver channel without any modification on traditional radar hardware. Compared with MUSIC algorithm which needs multiple receiver channels, the proposed strategy shows better performance with different setup about SNR level and target numbers. The improvement of the reconstruction performance when targets do not accurately lie in the discretized spatial grid of Ω is the future work.

Conflict of Interests

The authors declare that there is no conflict of interests regarding the publication of this paper.

Acknowledgments

The authors would like to thank Dr. Yinan Zhao for proofreading the paper and his valuable suggestions about the recovered procedure in the paper. This work was supported by the National Natural Science Foundation of China under Grant 61371181.

References

[1] E. J. Candes, J. Romberg, and T. Tao, "Robust uncertainty principles: exact signal reconstruction from highly incomplete frequency information," *Institute of Electrical and Electronics Engineers. Transactions on Information Theory*, vol. 52, no. 2, pp. 489–509, 2006.

[2] E. J. Candes and M. B. Wakin, "An introduction to compressive sampling," *IEEE Signal Processing Magazine*, vol. 25, no. 2, pp. 21–30, 2008.

[3] J. H. G. Ender, "On compressive sensing applied to radar," *Signal Processing*, vol. 90, no. 5, pp. 1402–1414, 2010.

[4] I. Bilik, "Spatial compressive sensing for direction-of-arrival estimation of multiple sources using dynamic sensor arrays," *IEEE Transactions on Aerospace and Electronic Systems*, vol. 47, no. 3, pp. 1754–1769, 2011.

[5] S. F. Cotter, "Multiple snapshot matching pursuit for direction of arrival (DOA) estimation," in *Proceedings of the 15th European Signal Processing Conference (EUSIPCO '07)*, pp. 247–251, Poznan, Poland, September 2007.

[6] A. Gretsistas and M. Plumbley, "A multichannel spatial compressed sensing approach for direction of arrival estimation," in *Proceedings of the 9th International Conference on Latent Variable Analysis and Signal Separation (LVA/ICA '10)*, pp. 458–465, St. Malo, France, 2010.

[7] J. Tropp, A. C. Gilbert, and M. J. Strauss, "Simultaneous sparse approximation via greedy pursuit," in *Proceedings of the IEEE International Conference of Acoustics, Speech and Signal Processing*, vol. 5, pp. 721–724, Philadelphia, Pa, USA, March 2005.

[8] E. van den Berg and M. P. Friedlander, "Theoretical and empirical results for recovery from multiple measurements," *IEEE Transaction on Information Theory*, vol. 56, no. 5, pp. 2516–2527, 2010.

[9] S. Ji, Y. Xue, and L. Carin, "Bayesian compressive sensing," *IEEE Transactions on Signal Processing*, vol. 56, no. 6, pp. 2346–2356, 2008.

[10] S. Ji, D. Dunson, and L. Carin, "Multitask compressive sensing," *IEEE Transactions on Signal Processing*, vol. 57, no. 1, pp. 92–106, 2009.

[11] G. Tzagkarakis, D. Milioris, and P. Tsakalides, "Multiple-measurement Bayesian compressed sensing using GSM priors for DOA estimation," in *Proceedings of the IEEE International Conference on Acoustics, Speech, and Signal Processing (ICASSP '10)*, pp. 2610–2613, Dallas, Tex, USA, March 2010.

[12] L. Gan, X. Q. Wang, and H. S. Liao, "DOA estimation of coherently distributed sources based on block-sparse constraint," *IEICE Transactions on Communications*, vol. 95, no. 7, pp. 2472–2476, 2012.

[13] M. Carlin, P. Rocca, G. Oliveri, F. Viani, and A. Massa, "Directions-of-arrival estimation through Bayesian compressive sensing strategies," *IEEE Transactions on Antennas and Propagation*, vol. 61, no. 7, pp. 3828–3838, 2013.

[14] J. M. Kim, O. K. Lee, and J. C. Ye, "Compressive MUSIC: revisiting the link between compressive sensing and array signal processing," *IEEE Transactions on Information Theory*, vol. 58, no. 1, pp. 278–301, 2012.

[15] X. Zhan, R. Zhang, D. Yin, and C. Huo, "SAR image compression using multiscale dictionary learning and sparse representation," *IEEE Geoscience and Remote Sensing Letters*, vol. 10, no. 5, pp. 1090–1094, 2013.

[16] X. X. Zhu and R. Bamler, "Tomographic SAR inversion by L1-norm regularization-the compressive sensing approach," *IEEE Transactions on Geoscience and Remote Sensing*, vol. 48, no. 10, pp. 3839–3846, 2010.

[17] E. J. Candès, Y. C. Eldar, D. Needell, and P. Randall, "Compressed sensing with coherent and redundant dictionaries," *Applied and Computational Harmonic Analysis*, vol. 31, no. 1, pp. 59–73, 2011.

[18] CVX Research Inc., "cvx toolbox," 2014, http://cvxr.com/.